Desalination 525 (2022) 115489

Contents lists available at ScienceDirect

Desalination

journal homepage: www.elsevier.com/locate/desal

Magnesium recovery from desalination reject brine as pretreatment for membraneless electrolysis

Nafis Mahmud [a], Daniela V. Fraga Alvarez [b], Mohamed H. Ibrahim [a], Muftah H. El-Naas [a,*], Daniel V. Esposito [b,c,d,**]

[a] Gas Processing Center, Qatar University, P.O. Box 2713, Doha, Qatar
[b] Department of Chemical Engineering, Columbia University in the City of New York, 500 W. 120th St., New York, NY 10027, United States of America
[c] Columbia Electrochemical Energy Center, Columbia University in the City of New York, 500 W. 120th St., New York, NY 10027, United States of America
[d] Lenfest Center for Sustainable Energy, Columbia University in the City of New York, 500 W. 120th St., New York, NY 10027, United States of America

HIGHLIGHTS

- Mg^{2+} recovery was evaluated as a pretreatment for membraneless electrolysis of desalination brine.
- Mg^{2+} recovery was optimized using response surface methodology.
- 98.8% Mg^{2+} recovery was achieved using 8.22 g/L NaOH at 45 °C.
- Mg^{2+} influence on the performance of the membraneless electrolyzer was assessed.
- The membraneless electrolyzer can tolerate up to 5 mM of Mg^{2+}.

ARTICLE INFO

Keywords:
Reject brine
Membraneless electrolyzers
Magnesium
Fouling
Optimization
Purification

ABSTRACT

Alkali-earth metals pose a significant challenge to water treatment technologies and electrochemical processes due to their propensity to precipitate as metal hydroxides, which can deposit on membranes and/or electrodes and reduce their efficiencies. Membraneless electrolyzers can partially overcome this issue because they lack membranes or diaphragms, however their electrodes are still susceptible to fouling. To overcome this issue, electrolyzers can be incorporated into a recirculating electrolyte scheme where magnesium is removed in the form of $Mg(OH)_2$ before reaching the electrolyzer. Motivated by this system, the first part of this study focuses on the optimization of magnesium recovery from desalination brine by adding NaOH using response surface methodology. Brine salinity, NaOH dose, and temperature were optimized with complete magnesium removal set as the target response using central composite design. Results showed that 98.8% of magnesium can be removed at brine salinity, NaOH dose, and temperature of 73.5 g/L, 8.22 g/L and 45.5 °C, respectively. The second part of this study investigated the influence of Mg^{2+} concentration on the performance of a cathode within a membraneless electrolyzer. Experimental demonstrations show that Mg^{2+} concentrations below 5 mM can be used as a feed stream without any noticeable build-up of $Mg(OH)_2$ deposits on the cathode surface over 3 h during electrolysis at 50 mA/cm^2. Finally, an analysis is presented to predict how long a cathode can operate in Mg^{2+}-containing electrolyte as a function of current density and superficial velocity of brine solution before the electrode reached its maximum tolerance of $Mg(OH)_2$ deposits.

1. Introduction

Significant water demand coupled with declining freshwater supplies is intensifying water scarcity worldwide. It is estimated that approximately 41% of the world's population suffers from water shortages [1]. Over the last few decades, desalination has become a large-

* Corresponding author.
** Correspondence to: D.V. Esposito, Department of Chemical Engineering, Columbia University in the City of New York, 500 W. 120th St., New York, NY 10027, United States of America.
E-mail addresses: muftah@qu.edu.qa (M.H. El-Naas), de2300@columbia.edu (D.V. Esposito).

https://doi.org/10.1016/j.desal.2021.115489
Received 30 August 2021; Received in revised form 25 November 2021; Accepted 30 November 2021
Available online 13 December 2021

scale technical solution to meet the ever-growing demands of freshwater, especially in water-stressed countries. Almost half of the desalination plants are located in the Middle East and North Africa, accounting for 48% of the global desalination capacity [2]. Desalination plants use large volumes of seawater and discharge concentrated water (reject brine) back to the environment. Brine production is usually equivalent to or greater than the total volume of the desalinated water. The disposal of reject brine is becoming a major economic and environmental concern due to its elevated salinity and temperature as well as chemical additives added during its pretreatment [3]. There are several brine management approaches depending on disposal cost and regulations, geographic or physical location of the discharge point, and brine volumes [4]. Most of these approaches focus on direct disposal and management rather than treatment and reuse. They can also be costly, energy-intensive, and could have detrimental effects on the environment. These approaches include brine evaporation, concentration, crystallization, and distillation [1–3]. Desalination plants often dispose of reject brine into the close-by surface water bodies like the sea or the ocean [4]. The long-term impact of brine disposal operations on marine environment is still unknown, but the high temperature and salinity associated with reject brine may have harmful effects on marine life. Nonetheless, instead of disposing of the brine, its metals and ions content can be harvested and used to produce chemicals with high commercial value. Mavukkandy et al., recently reviewed thermal and membrane-based techniques to recover valuable materials from the reject brine [5]. Among these techniques, electrochemical conversion stands out as a means of producing sodium hydroxide (NaOH) from reject brine through the use of membrane-based electrodialysis cells or chlor-alkali electrolyzers.

The electrodialysis with bipolar membranes (EDBM) generates a stream of alkaline and acidic effluent containing NaOH and hydrochloric acid (HCl). EDBM can be challenging for large-scale production of acid and base from reject brine due to the susceptibility of membranes to degradation and fouling, especially in the presence of impurities. Although the electrodes in an EDBM might not be directly exposed to impurities from the reject brine, thanks to shielding from the membranes, the membranes themselves can be susceptible to fouling and degradation. In general, fouling is a major issue in membrane processes/units and often represents a major challenge for membrane desalination processes [6,7]. In particular, the challenge of stabilizing anion exchange membranes, an essential half of the bipolar membrane, has been openly recognized for applications involving seawater [8]. Another challenge is the sodium hydroxide production capacity of the EDBM. It has been reported in the literature that the EDBM technology can produce NaOH concentration from brine between 0.2 and 2.4 M compared to a commercially required concentration of 18.9 M [9].

An alternative electrochemical process for generating sodium hydroxide from brine is conventional brine electrolysis carried out in a chlor-alkali electrolyzer [10]. Although the Chlor-Alkali process is the industrial standard for cost-effective production of NaOH, it requires high brine purity to avoid membrane fouling. In addition, the chlor-alkali process generates large amounts of toxic Cl_2 [11,12]. Unlike the above-mentioned electrochemical processes, membraneless electrolyzers do not require a membrane between the anode and cathode. In addition, they can operate at large current densities (>100 mA/cm^2) compared to EDBM units which often operate with current densities between 5 mA/cm^2 to 10 mA/cm^2. This difference in current density translates to a higher throughput of reactants/products per unit area of the device, meaning that a much smaller (i.e., lower cost) device can be utilized if it can operate at higher current density, with all else being equal. While low current may not be a problem from an operational standpoint, it will have an effect on the capital costs of the system [13].

Membraneless electrolyzers depend on the separation of products by fluid flow [14] and/or buoyancy of gaseous products [15]. By removing the membrane, the electrolyzers have the potential to be highly durable under challenging conditions, as they do not experience membrane fouling. Theelectrolyzer considered in this work are based on porous flow-through electrodes for which the electrolyte is continuously pumped through the pores in the electrodes during operation. However, scales formed by the precipitation of magnesium and calcium hydroxides can deteriorate the performance of the electrode, as they can block the electrochemical active sites [15]. In general, brine contains considerable amounts of magnesium (Mg^{2+}) and calcium (Ca^{2+}) ions. Hence, removing these ions is essential for the long-time durability of the electrodes. This study proposes to achieve this goal through the process scheme illustrated in Fig. 1, where alkalinity produced from the cathode effluent of a membraneless electrolyzer such as those previously reported [13,16], is used to drive the chemical conversion of Mg^{2+} and Ca^{2+} ions into hydroxides and/or carbonates. Within this process, the alkaline effluent from the membraneless electrolyzer is recirculated back towards the inlet of the electrolysis process such that it can be used to facilitate the removal of the alkali earth metal ions as solid precipitates before they have a chance of reaching the electrolyzer. By this means, the proposed scheme provides a means of harvesting valuable solid carbonates and/or hydroxides while potentially preventing these minerals from depositing on the cathodes of the electrolyzer.

Consistent with the basic idea illustrated in Fig. 1, several previous studies have discussed the removal of magnesium from brine using different alkaline agents. Mohammad et al. recovered 99% of magnesium at high brine salinity and low temperature using ammonia. The authors reported high purity of the recovered magnesium in the form of magnesium hydroxide [17]. Similarly, Dong et al. used ammonium hydroxide and sodium hydroxide to precipitate magnesium hydroxide for the subsequent production of magnesium oxide (MgO) to be used as a cement binder. They reported that the type of reagent used can influence the textural properties, reactivity, and microstructure of the produced MgO. The ammonia-based MgO had a more porous structure compared to sodium hydroxide-based MgO. Nonetheless, the use of ammonia can be a major concern, as it is considered an environmental and health hazard that can lead to respiratory failure. Ruan et al. investigated the production of magnesium oxide from reject brine by adding sodium hydroxide/magnesium at a molar ratio of two and reported that MgO produced can be used as an effective cement binder for construction applications [18]. In this work, reject brine obtained from a local desalination plant was treated with NaOH to remove magnesium in the form of magnesium hydroxide. Response surface methodology was used to determine the optimum conditions for maximum magnesium recovery by varying three experimental parameters including brine salinity (S), NaOH (N), and temperature (T). Mg^{2+}-containing electrolyte was fed to a membraneless electrolyzer and its capability to simultaneously produce acid and base in the presence of Mg^{2+} was evaluated. Overpotential losses were measured at varying concentrations of Mg^{2+} in brine to determine maximum allowable deposits of $Mg(OH)_2$ on the surface of the cathode before the device is too inefficient to operate. To the best of the authors' knowledge, such inclusive optimization has not been reported in the open literature.

2. Methods

2.1. Thermodynamic analysis of the reaction

The magnesium ions in the reject brine samples are usually present in the form of carbonates, chlorides, or sulfates. The addition of sodium hydroxide elevates the pH of brine solution leading to the precipitation of the magnesium ions into magnesium hydroxide [17], as shown by the reaction (1):

$$2NaOH\ (aq.) + Mg^{2+}\ (aq.) \leftrightarrow 2Na^{+}\ (aq.) + Mg(OH)_2\ (s) \quad (1)$$

The thermodynamics of this reaction was then evaluated using the reaction equations tool of HSC chemistry software [19]. Using this tool, the heat of reaction and Gibbs free energy (ΔG) was calculated over a

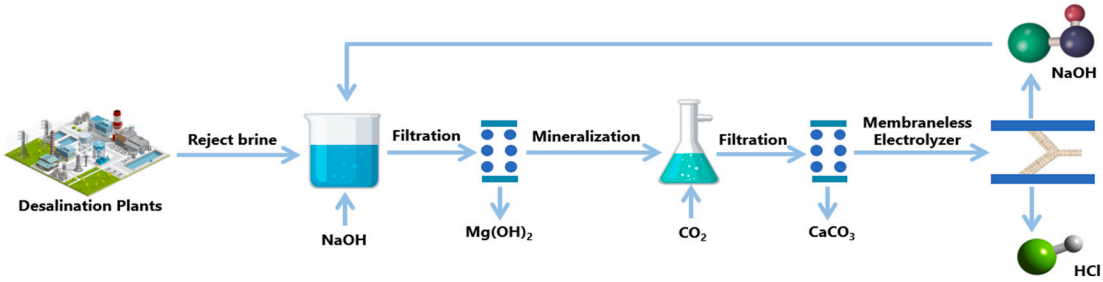

Fig. 1. A simplified process flow diagram illustrating the removal of alkali earth metal ions from desalination reject brine reaching a membraneless electrolyzer used for producing dilute base and acid from the brine solution.

temperature range of 0 to 100 °C with increments of 10 °C. The results indicated that the reaction exhibited a negative change in enthalpy (ΔH) and ΔG at the given temperature range. The former is an affirmation of the reaction being exothermic in nature, while the latter affirms that the reaction is spontaneous over the entire range (Fig. 2).

2.2. Reject brine characterization

The reject brine samples used to perform this study were obtained from a local water desalination plant located in Doha, Qatar, which utilizes a multi-stage flash (MSF) distillation process. The reject brine samples were collected from the last stage of the aforementioned MSF process and the characteristics of the obtained reject brine are provided in Table 1. The concentrations of all the major cations and anions were determined using Shimadzu 9800 inductively coupled plasma atomic emission spectroscopy (ICP-OES) and Metrohm 850 Professional ion chromatography (IC), respectively. The ICP-OES analysis indicated that sodium, potassium, calcium, and magnesium were the major cations and the IC analysis confirmed bromine, sulfate, and chloride were the major anions present within the brine samples. Hach TNT 822 reagents were used to determine the chemical oxygen demand (COD) of the samples in a Hach DR 3900 UV spectrophotometer. The pH and conductivity of the samples were determined using Thermo Scientific Orion Star A325 meter. The total dissolved solids (TDS) method was carried out following the standard APHA 2540 °C method at room temperature. Furthermore, the method was also used to determine the correlation (Fig. 3) between the conductivity and salinity of reject brine samples at room temperature [20].

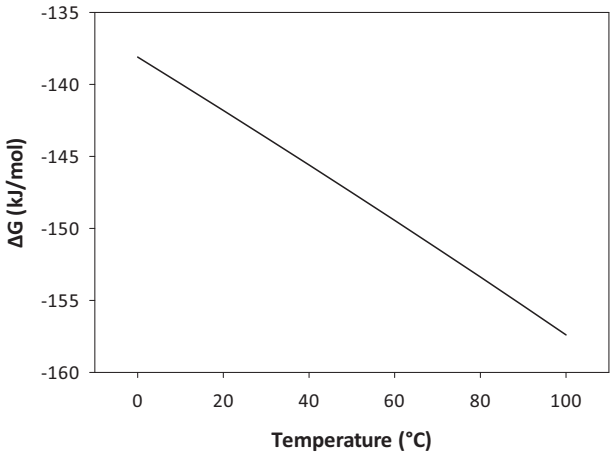

Fig. 2. Gibbs free energy (−ΔG) versus temperature as calculated by HSC software for reaction (1).

Table 1
Characteristics of the obtained reject brine.

Parameters	Value
Sodium (mg/L)	24,299
Potassium (mg/L)	1094
Calcium (mg/L)	837
Magnesium (mg/L)	2879
Bromide (mg/L)	106
Sulfate (mg/L)	5497
Chloride (mg/L)	40,444
TDS (mg/L)	76,200
COD (mg/L)	2270
Conductivity (mS/cm)	93.5
pH	8.9

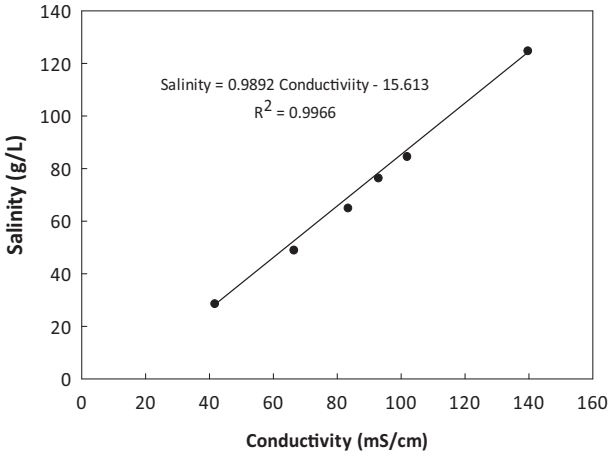

Fig. 3. Relationship between salinity and conductivity determined from reject brine samples at room temperature via TDS at the standard APHA 2540 °C method.

2.3. Screening experiments

Initially, screening experiments were performed to determine the effects of various process parameters, namely Salinity (S), amount of NaOH (N) and reaction temperature (T) on the efficiency of magnesium ions removal. Based on these experiments, applicable ranges for each individual parameter (Table 3) were selected for developing an experimental design to apply response surface methodology (RSM). All the experiments were performed using the original brine samples. The salinity of the experimental runs was varied between 23.9 and 123.1 g/L, thus, varying the initial magnesium content of the brine samples as given in Table 2. To increase or decrease the salinity, the original brine samples were concentrated via evaporation or diluted with DI water, respectively. The amount of sodium hydroxide added was varied between 1 and 14 g/L, and the temperature was varied between 18 and

Table 2
Brine salinity and its corresponding magnesium content.

Salinity (g/L)	Magnesium (mg/L)
Original reject brine feed	2879
23.0	1099
44.0	1789
73.5	2689
103	3819
123	4789

45 °C. This range was selected in keeping with the temperature at which the brine is rejected at the local desalination plant. For each experimental run, around 100 mL of reject brine of a given salinity was transferred to a conical flask and a specific amount of NaOH (Purity 98.5% Sharlab) was added. The flask was then placed inside a temperature-controlled shaker (Labnet model), where it was mixed very well at 200 RPM for 2 h. The samples were then filtered using Restek 13 mm 0.45 μm (Nylon) syringe filters and analyzed using ICP-OES. The amount of magnesium removed was then calculated using Eq. (2).

$$Mg\ Removal\% = \frac{C_i - C_f}{C_i} \quad (2)$$

where, C_i and C_f represents the initial and final magnesium concentrations (mg/L) of the feed brine sample, respectively.

2.4. Experimental design using response surface methodology

Response surface methodology or RSM is a method that can be used to interpret the behavior of set of experimental data by generating a second order model representing the experimental data [21,22]. Statistical assessments are then made to determine the accuracy of the obtained second-order model. The model can be further used to optimize and tune a system's output to attain the desirable outcome [23,24]. Minitab 19 software was used to formulate an experimental design using RSM based on the applicable range attained from the initial experimental screenings of the process variables (S, N, and T). The software was then used to analyze and fit the experimental data to a regression model through central composite design (CCD) as given by Eq. (3).

$$Y = \beta_0 + \sum_{i=1} \beta_i X_i + \sum_{i=1} \beta_{ii} X_i^2 + \sum_{i=1} \sum_{J=i+1} \beta_{ij} X_i X_j \quad (3)$$

where Y, β_0, β_i, β_{ii}, β_{ij}, X_i, and X_j represent the response function, offset term, linear effect coefficient, squared effect coefficient, interaction effect coefficient, variable value with code *i*, and variable value with code *j*, respectively [25]. Afterwards, the Minitab optimizer tool was used to optimize the three process parameters (S, N, and T) for a target response, which in this work was set to be as 100% recovery of magnesium. The goodness of the optimization in RSM can be evaluated based on desirability parameter. The desirability value is usually between 0 and 1, where a desirability value close to 1 indicate the target response close to the ideal value.

2.5. Characterization of solid products

After determining the optimum conditions for brine salinity, NaOH dose and Temperature via the Minitab optimizer output, experiments were carried out under those conditions and the obtained precipitates were collected for further analysis. At first, the solid precipitates were separated using centrifuge and redispersed in deionized water followed by another step of centrifugation. After five alternative cycles of centrifugation and redispersion in deionized water, the solid products were separated and kept for drying overnight in an oven at 105 °C. X-ray diffraction analysis of the solid samples were then carried out using a Rigaku Miniflex II at operated at 40 kV using a Cu Kα radiation (λ = 1.5406 Å) within a 2θ range of 5° to 80°. Thermogravimetric analysis of the solid samples were carried out using a Perkin Elmer TGA (Model: Pyris 1) under nitrogen environment in the temperature range of 30–1000 °C with a heating rate of 10 °C/min. The temperature ranges where noticeable weight loss occurred were used to detect the possible products along their purity. Finally, the Energy Dispersive Spectra (EDS) analysis of the samples were carried out using Thermofisher Qunta 200 to identify and determine mass of various elements present within the solid samples.

2.6. Fabrication of membraneless electrolyzers

2.6.1. Electrode fabrication

The anode was fabricated by cutting titanium (Ti) foil (0.127 mm, annealed, 99% metal basis, Alfa Aesar) into a 1 cm × 7 cm rectangle (see Fig. S1a) and depositing 50 nm of platinum (99.99%) via electron-beam evaporation at a rate of 1 Å/s. A portion of the fabricated electrode measuring 1 cm × 2 cm was inserted into the cell and the protruding Ti foil was used to establish an electrochemical connection. To fabricate the cathode, porous conductive carbon foam characterized by 100 pores per inches (PPI) and sheet resistance of 7.87 × 10–2 Ω/sq (McMaster-Carr) was cut into a 1 cm × 4.5 cm rectangle. A segment of the electrode measuring 1 cm × 2 cm and 1 cm × 2.5 cm was sliced to a thickness of 0.32 cm and 0.5 cm, respectively. Titanium foil measuring 0.8 cm × 2 cm was used as the electrical feedthrough and inserted into the thicker portion of the electrode (see Fig. S1b). Before platinization of the carbon foam, the substrate was first sonicated in isopropanol, methanol, and DI water for 5 min each followed by a two-step chronoamperometry (CA) to remove impurities from the surface in deaerated 0.5 M H_2SO_4 electrolyte. The CA pretreatment was carried out using potentials of 0.4 V vs. Ag|AgCl and −0.8 V vs. Ag|AgCl for 5 s each for a total of 10 s. Electrodeposition of the platinum electrocatalyst was then conducted in deaerated 3 mM K_2PtCl_4 + 0.5 M NaCl electrolyte (pH = 2.60) by running cyclic voltammetry (CV) between −0.7 V vs. Ag/AgCl and 0.3 V vs. Ag/AgCl for 21 cycles at 100 mV/s. The electrochemically active surface area (ECSA) of cathodes used in this work was typically 26–37 cm^2 per cm^2 of geometric area, determined by integration of the underpotential hydrogen features in the last CV curve based on a specific capacitance of 210 μC/cm^2 for polycrystalline Pt. [26] Scanning electron microscopy (SEM) images of the Pt nanoparticles electrodeposited onto carbon foam electrodes were recorded using a Zeiss Sigma VP Scanning Electron Microscope.

2.6.2. Design of membraneless electrolyzer

The electrolyzer was designed in Autodesk ® Inventor and 3D printed in a MakerGear M3-ID 3D printer using Acrylonitrile Butadiene Styrene (ABS) as the filament material and 100% solid infill. ClearWeld, J.B Weld epoxy was used to secure glass windows, comprised of glass microscope slides, and the electrodes within the electrolyzer chassis. The design file for the electrolyzer has been made freely available on echem.io.

A Biologic SP 200 potentiostat was used to perform all the electrochemical experiments. The electrolyzer inlet and outlets were connected to the electrolyte reservoir and effluent collection beakers, respectively, using silicon tubing (Masterflex L/S, Cole-Parmer). The device was mounted in a vertical position, with the feed stream entering the bottom of the device and effluent streams leaving the top of the device. Peristaltic pumps (NE-9004, Peristaltic Pump) were connected to each of the effluent tubes and used to draw the anode and cathode effluent streams into glass collection beakers. The pH of the collected effluent streams was measured with a Benchtop pH meter (Fisher Scientific), which was calibrated using pH 4.01, 7.00, and 12.46 standard buffer solutions (Oakton Buffer Solution, Cole-Parmer). The feed reservoir was constantly purged with nitrogen (N_2, Purity Plus 99.999% purity) at 1 atm during the experiments to remove the oxygen.

2.7. Testing the magnesium tolerance of membraneless electrolyzers

All solutions were prepared using 18.2 MΩ-cm deionized water. Electrolytes were prepared using sulfuric acid (Certified ACS plus, Fisher Scientific), sodium chloride (Certified ACS, Fisher Scientific), magnesium chloride (≥98% anhydrous Sigma Aldrich), and hydrochloric acid (Certified ACS Plus, Fisher Scientific).

A dedicated cell was used for each solution containing a different concentration of $MgCl_2$. First, deaerated 0.5 M H_2SO_4 (pH ≈ 0.9) was fed into the cell at 10 mL/ min and CV cycling was carried out between −0.09 V vs. RHE to 1.2 V vs. RHE at 50 mV/s for 38 cycles to evaluate the ECSA. The electrode performance towards the hydrogen evolution reaction (HER) was evaluated in 1 M NaCl with and without the presence of magnesium. For a given 1 M NaCl + X mM (X=0 mM, 1.2 mM, 5 mM, or 120 mM) $MgCl_2$ solution, the initial series resistance was measured by electrochemical impedance spectroscopy (EIS) using a frequency range of 200 Hz to 100 mHz and an AC amplitude of 10 mV at 0 V vs. RHE in a stagnant electrolyte. To evaluate the initial electrode performance towards the HER, 5 CV cycles were recorded from +0.2 V vs. RHE to −1.0 V vs. RHE at 50 mV/s. Next, chronopotentiometry (CP) measurements were carried out at a constant current density of 50 mA/ cm^2 for 3 h. The pH values of the anodic and cathodic effluent streams were measured after 45, 105, and 165 min of operation. After CP measurements, the series resistance of the cell was again measured by EIS, and CV curves were recorded using the same parameters given above.

3. Results and discussion

3.1. Response surface model optimization

The RSM optimization of the three process variables, namely salinity (29.9–123.1 g/L), NaOH (1.28–14.7 g/L), and temperature (18.6–45.5 °C) was carried out at the highest and lowest levels of +1 and −1, respectively. The target response of the RSM was set to be 100% magnesium removal. The required experimental conditions for 20 experimental runs based on the central composite design along with the obtained experimental response and predicted response are listed in Table 4. From Table 4, it can be observed that complete removal of magnesium (100%) was achieved for 5 of the 20 experimental runs. The lowest magnesium removal (17.2%) was observed at brine salinity, NaOH dose and temperature of 73.5 g/L, 1.28 g/L, and 32 °C, respectively. The second-order regression model representing the percentage of magnesium removal as a function of the three studied process variables and in terms of all the factors is given by Eq. (4).

$$\begin{aligned}\text{Magnesium removal}\% = {} & 27.3 + 0.113\ \text{S} + 13.24\ \text{N} + 0.232\ \text{T} - 0.007608\ \text{S*S} \\ & - 0.8557\ \text{N*N} - 0.0012\ \text{T*T} + 0.08399\ \text{S*N} \\ & - 0.00125\ \text{S*T} - 0.0006\ \text{N*T}\end{aligned} \quad (4)$$

ANOVA analysis of the response surface model was carried out for magnesium removal in terms of the selected process parameters. The significance of any given process parameter was determined by the *P*-value. Any factor exhibiting a P-value <0.05 was deemed to be significant for the target response, while for a *P*-value >0.05 it was considered to be insignificant. Based on this hypothesis, the second-order polynomial model in terms of significant factors can be reduced to Eq. (5):

$$\begin{aligned}\text{Magnesium removal}\% = {} & 27.3 + 0.113\ \text{S} + 13.24\ \text{N} - 0.007608\ \text{S*S} \\ & - 0.8557\ \text{N*N} - 0.08399\ \text{S*N}\end{aligned} \quad (5)$$

3.2. Process optimization

Minitab's response surface optimizer was used for the optimization of the three process parameters with a target response of 100% magnesium removal. Based on the output of the optimizer, optimum conditions for salinity, NaOH and Temperature was found to be as 73.5 g/L, 8.22 g/L, and 45.5 °C, respectively. The obtained optimizer output was compared to the work of Dong et al. [27,28], where the optimum molar ratio for $NaOH/Mg^{2+}$ was reported to be around 2 for 94–99% removal of magnesium. The optimum molar ratio for $NaOH/Mg^{2+}$ based on the optimizer output was found to be around 1.85 for the complete removal of magnesium. Thus, the findings of the RSM can further reduce the operating cost for complete removal of magnesium from reject brine. Moreover, a desirability value of 1 was obtained for the model which shows the closeness of the response to the target response as well as the applicability of the response surface model for the magnesium removal.

3.3. Model validation

The accuracy of the obtained response surface model was verified by comparing the experimental response (i.e., Magnesium Removal %) against the predicted response as shown in Fig. 4. It is evident that the obtained experimental values, represented by scattered points, are very close to the diagonal line representing the predicted response, thereby, indicating a linear behavior. Moreover, the obtained R^2 value of 0.9941 between the two responses also signifies an excellent fit for the response surface model.

To further evaluate the validity of the RSM, additional experiments were conducted at a few random conditions as well as at the optimum conditions for Salinity, NaOH and temperature. The obtained response from these experiments was compared to the predicted response based on the generated regression model via RSM (see Table 5). It was evident that the experimental Mg removal under random experimental conditions was close to the predicted response and within the 95% confidence interval. A similar trend was observed in case of the experiments conducted at the optimal conditions. These findings elucidate the validity and competency of the response surface model to predict the removal of Mg from brine at given conditions.

3.4. Effect of process variables on magnesium removal

3D surface plots were generated using the regression model to understand the effect of interactions between the three process parameters (Salinity, NaOH and temperature) on magnesium removal. The plots were generated by keeping one of the process variable constant while varying the other two as shown in Fig. 5. Based on the observations of Fig. 5 and experimental runs of Table 3, the effect of each individual parameter on the removal of magnesium is discussed in the following sections.

3.4.1. Effect of NaOH

The effect of the interactions between NaOH dosage with the other

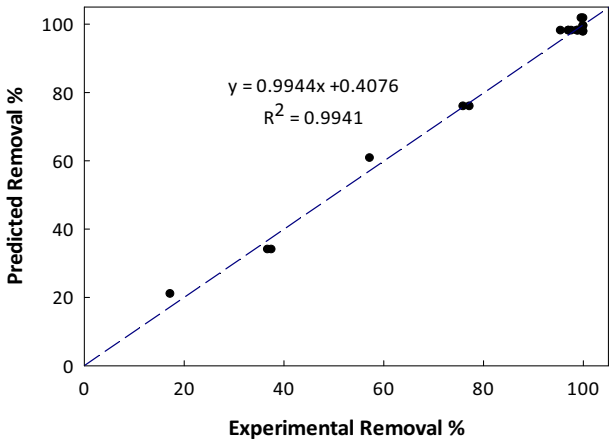

Fig. 4. The experimental vs predicted values for magnesium removal based on response surface design.

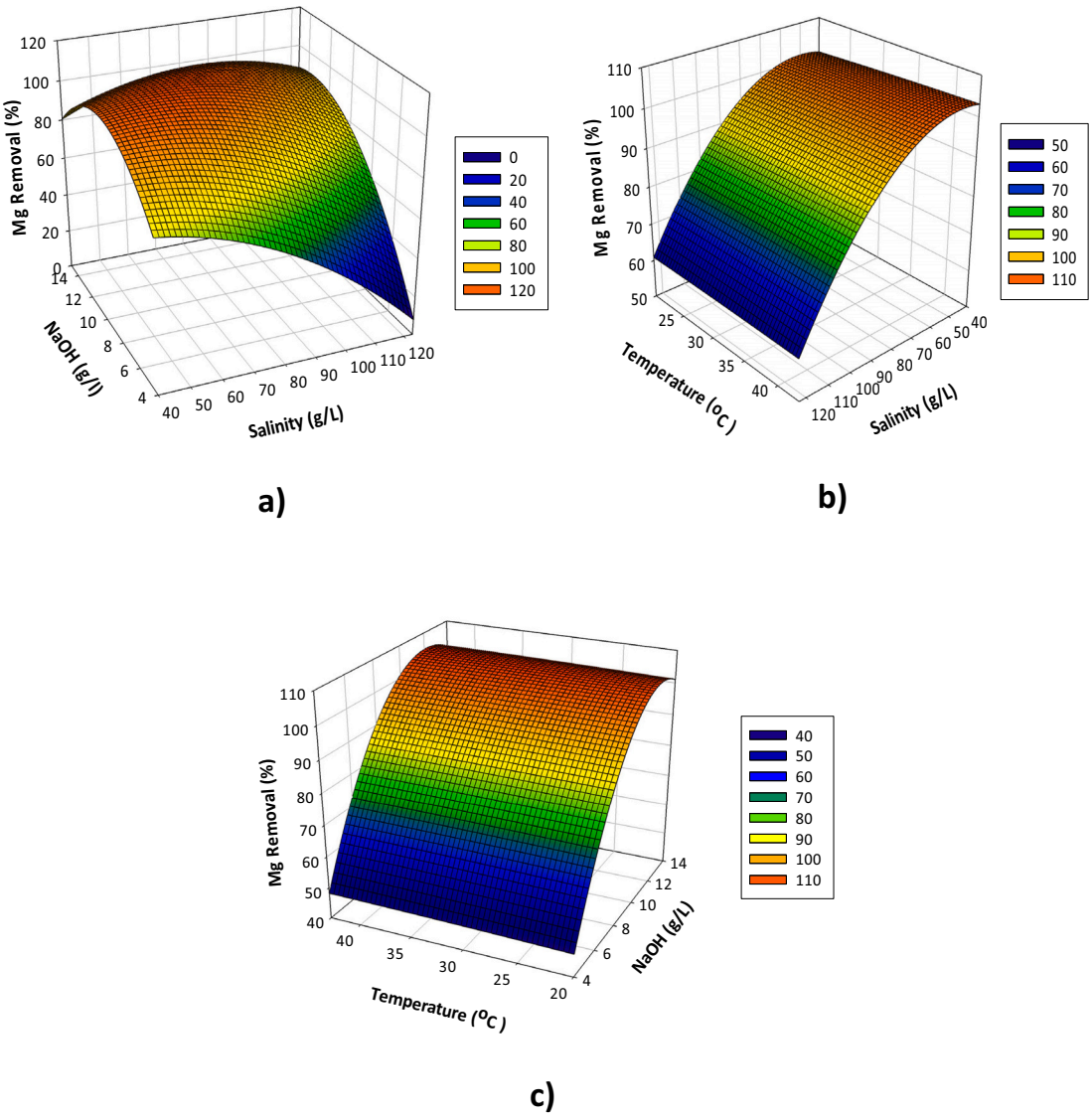

Fig. 5. 3D plots of interaction effect of the process parameters on Magnesium Removal (a. NaOH vs Salinity at constant temperature of 32°C, b. temperature vs salinity at constant NaOH dose of 8 g/L and c. temperature. vs NaOH at constant salinity of 73.5 g/L) based on the regression model.

Table 3
Range and level of the variables for central composite design runs.

Process parameter	Code	Levels				
		−α	−1	0	+1	+α
Salinity (g/L)	S	23.9	44.0	73.5	103.0	123.1
NaOH (g/L)	N	1.3	4	8	12	14.7
Temperature (°C)	T	18.6	24	32	40	45.5

two process parameters, namely, salinity and temperature on the removal of magnesium are shown in Fig. 5a and b, respectively. At a constant salinity of 103 g/L, a temperature of 24 °C, and NaOH dose of 4 g/L showed 37.5% removal of magnesium. Under the same conditions, increasing the NaOH dose to 12 g/L resulted in the complete removal of magnesium (62.5% increase). Similar behavior was also observed at a constant salinity of 73.5 g/L and temperature of 32 °C, where an increase of NaOH dose from 1.28 g/L to 8 g/L resulted in an approximately 80% increase in magnesium removal. This behavior was mainly caused by the availability of more hydroxyl ions with the increase of NaOH dosage, which in turn drives magnesium ions present within the brine to form more solid magnesium hydroxide products [27]. It is worth noting that complete removal of magnesium was observed at NaOH dose of 12 g/L or more regardless of the salinity. Since at high NaOH dosage, the amount of sodium hydroxide exceeded the stoichiometric ratio (2:1) required for the reaction between NaOH and Mg^{2+} as observed in Eq. (1). Upon observing the Fig. 4a, it can be observed that there is an optimum dose for NaOH for Mg removal which was determined by the Minitab optimizer as 8.22 g/L.

3.4.2. *Effect of salinity*

Fig. 5a and c shows the effect of interactions between brine salinity with NaOH dosage and temperature, respectively. At a constant NaOH dose of 4 g/L and temperature of 24 °C, the increase of brine salinity from 44 to 103 g/L caused a decrease in magnesium removal from 76.0 to 37.5%. Brine salinity of 23.89 g/L showed complete removal of magnesium at a constant NaOH dose of 8 g/Land temperature of 32 °C. A negligible reduction in magnesium removal was observed at salinity of 73.5 g/L, however, increasing the salinity to 123.1 g/L reduced the removal efficiency to 57.2%. This behavior was mainly caused by the increase in the magnesium content of brine with increase in brine salinity (Table 2), consequently requiring a higher NaOH dose for complete magnesium removal. Based on the output of Minitab

Table 4
Central composite design experimental runs with predicted Response.

Run	Salinity (g/L)	NaOH (g/L)	Temperature (°C)	Magnesium removal (%)	
				Experimental	Predicted
1	73.5	8	18.6	95.5	97.1
2	73.5	8	32	99.1	98.1
3	23.9	8	32	100.0	98.0
4	73.5	8	32	98.8	98.1
5	73.5	8	32	97.6	98.1
6	103.0	4	40	36.8	34.2
7	73.5	8	32	97.1	98.1
8	73.5	1.3	32	17.2	21.0
9	73.5	8	32	99.7	98.1
10	44.0	12	40	100.0	100.0
11	103.0	12	40	100.0	99.6
12	73.5	14.7	32	100.0	97.8
13	103.0	12	24	100.0	99.3
14	73.5	8	32	97.1	98.1
15	123.1	8	32	57.2	60.8
16	73.5	8	45.5	98.8	98.7
17	44.0	4	40	77.2	76.6
18	44.0	4	24	76.0	75.1
19	103.0	4	24	37.5	33.8
20	44.0	12	24	99.6	100.0

optimizer, the optimum salinity for this process was at 73.5 g/L. Since, this value of salinity is similar to that of the reject brine obtained from the MSF process [17,29], complete removal of magnesium can be achieved without any pretreatment step.

3.4.3. *Effect of temperature*

Similarly, the effect of interaction relation between Temperature with NaOH dose and Brine Salinity on Magnesium removal was investigated by Fig. 5b and c. It can be clearly seen that the temperature had no significant effect on the magnesium removal. This was caused by the fact that within the experimental temperature range (18–45 °C), salinity remains unaffected resulting in no change in magnesium content. On the other hand, NaOH being a non-volatile base, shows relatively low mass loss within the experimental temperature range. Therefore, the magnesium removal observed in Fig. 5b and c is being triggered by NaOH dose and Brine salinity. However, based on the optimizer output, the optimum condition for temperature was found to be 45 °C, which is highly desirable as it is close to the temperature at which the brine is rejected from the MSF process [30].

3.5. *Characterization of the solid products at optimum reaction conditions*

The solid precipitate obtained from the experimental run conducted at 73.5 g/L of brine salinity, 8.22 g/L of NaOH dose and 45.5 °C Temperature was collected and subsequently treated following the methodology outlined in Section 2.5. The solid products collected were expected to contain magnesium hydroxide, were subsequently characterized using various techniques. Fig. 6 shows the X-Ray diffraction (XRD) analysis of the recovered solid samples at optimum conditions. The XRD pattern comprised of the characteristic peaks of magnesium hydroxide [JCPDS No. 7-0239] as indicated by the peaks noticed at 2θ values of 18.6°, 33.1°, 38.2°, 51.0°, 58.8°, 62.4°, 68.7°, and 72.3° corresponding to the (001), (100), (101), (102), (110), (111), (103), and (201) planes, respectively [17,27,31]. In addition to these peaks, the minor peak observed at 29.7° in the XRD pattern confirms the presence of small amounts of calcium carbonate in the recovered $Mg(OH)_2$ samples.

The EDS analysis of the solid samples at three different areas further confirmed the presence of magnesium and oxygen as the main elements of the solid samples with small amounts of calcium. Based on the analysis, the average mass percentage of Mg and O accounted for 97% of the total mass with calcium serving as the balance. The thermal characteristics of the obtained solid products were also investigated using TG/DTA as shown in Fig. 7 where two endothermic peaks were detected. The first peak was observed between the temperature range of

Table 5
Experimental runs for validation of CCD design.

Experimental conditions	Salinity (g/L)	NaOH (g/L)	Temperature (°C)	Experimental Mg removal (%)	Predicted Mg removal (%)	95% confidence interval
Random	40.7	1.6	45	50.9	49.5	39.3–59.7
	56.5	2.8	30	53.7	56.8	53.0–60.6
Optimum	73.5	8	45.5	98.8	100	97.9–100

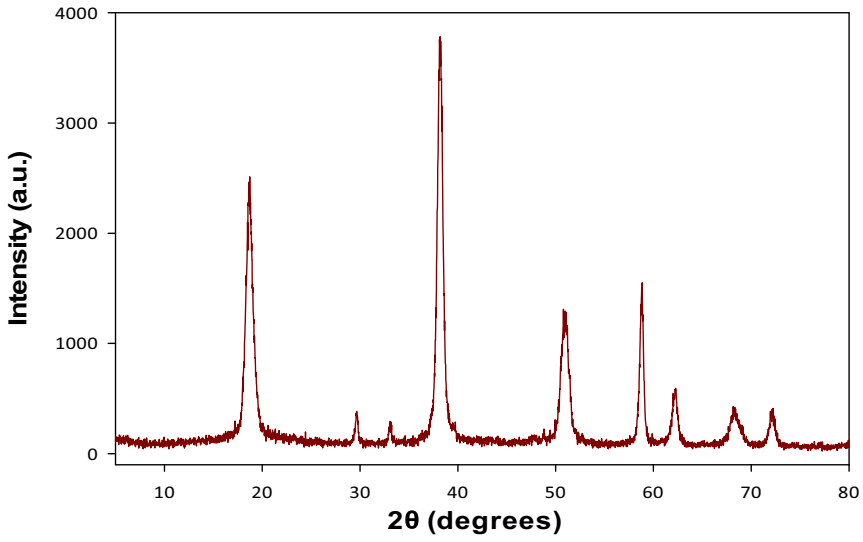

Fig. 6. XRD pattern of the $Mg(OH)_2$ recovered at brine salinity of 73.5 g/L, NaOH dose of 8.22 g/L, and temperature of 45.5 °C.

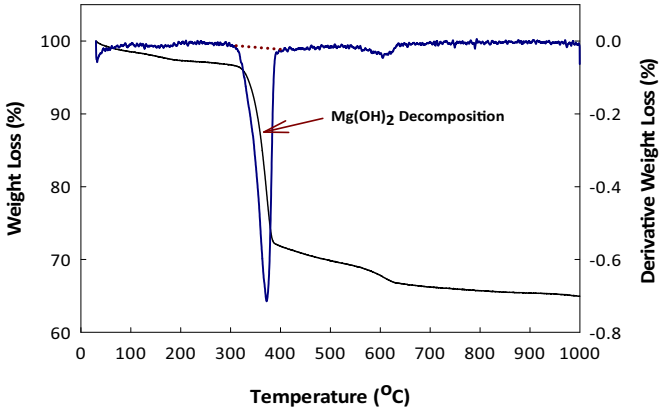

Fig. 7. The TG/DTA analysis of the recovered $Mg(OH)_2$ at brine salinity of 73.5 g/L, NaOH dose of 8.22 g/L and a Temperature of 45.5 °C.

350–400 °C, causing an overall weight loss of 24.5%. This loss can be explained by the decomposition of the magnesium hydroxide into magnesium oxides, as reported by several studies [32–36]. The weight loss was also indicative of the purity of the recovered magnesium hydroxide at optimal conditions. Pure magnesium hydroxide reportedly exhibits a weight loss of around 30.9% [37], which is slightly higher than the recovered $Mg(OH)_2$. A second endothermic peak was observed beyond 550 °C causing a further weight loss of 2% that can be attributed to the de-carbonation of calcium carbonate present within the samples [18]. Overall, based on the XRD, EDS and TG/DTA analysis it can be confirmed that the high purity magnesium hydroxide can be obtained as the final product under the optimum conditions for the response surface model.

3.6. Impact of Mg^{2+} on the performance of a membraneless electrolyzer

Having established the ability to precipitate and harvest Mg as $Mg(OH)_2$ from brine, it is essential to examine the ability of a membraneless electrolyzer to tolerate dissolved Mg^{2+} in the feed brine. Motivated by brine treatment applications, a study of membraneless electrolyzers capable of performing water electrolysis in an unbuffered brine solution was conducted. Large pH gradients are created between the anode and cathode effluent streams due to the oxygen and hydrogen evolution reactions, respectively, which are given by Eqs. (6) and (7):

$$2H_2O + 2e^- \rightarrow H_2 + 2OH^- \quad (6)$$

$$4OH^- \rightarrow O_2 + 2H_2O + 2e^- \quad (7)$$

As previously described by Talabi et al. [13], membraneless electrolyzers can leverage the principle of flow-induced separation to produce alkaline and acidic effluent streams based on Eqs. (6) and (7), respectively. Moreover, the pH of the effluent streams can be varied depending on the current density and volumetric flow rate of electrolyte passing through the electrolyzer. For the cathode effluent stream, pH varies according to:

$$pH_{cathode} = 14 + log_{10}\left[\frac{\gamma_{OH^-}\, i\, A_e \xi_c}{(v_c) n_c F}\right] \quad (8)$$

where γ_{OH^-} is the activity coefficient ($\gamma_{OH^-} = 0.86$), i is the applied current density (50 mA/cm^2), A_e is the 2D area of the electrode (2 cm^2), ξ_c is the current utilization, v_c is the flow rate of the cathodic effluent stream (5 mL/min for all experiments in this work), n_c is the stoichiometric number of electrons for the cathodic (reduction) reaction, and F is the Faraday constant. Acidic and alkaline streams generated based on Eqs. (6) and (7) can be useful for a wide range of processes. However, a major challenge of carrying out HER within the reject brine solution is the presence of Mg^{2+}, which can precipitate according to Eq. (1) to form solid magnesium hydroxide ($Mg(OH)_2$) that can deposit onto the cathode surface [38–40]. These deposits can subsequently reduce the performance of the cathode by creating an added ohmic resistance and by blocking electrocatalyst active sites. Thus, it is necessary to reduce the concentration of Mg^{2+} in the brine fed to the electrolyzer based on a scheme such as that shown in Fig. 1.

To evaluate the tolerance of cathode operation to the presence of Mg^{2+} ions, platinized carbon foam cathodes and platinized Ti foil anodes were fabricated and incorporated into a membraneless electrolyzer test platform in a face-to face configuration as shown in Fig. 8. The porous cathode was inserted through an opening in the cell chassis. A Ag|AgCl reference electrode was placed perpendicular to the cathode such that the end of the reference electrode was positioned next to the upstream edge of the cathode. Within this design, the porous flow-through cathode was studied as the working electrode while the platinized titanium foil served as the counter electrode. During operation, two peristaltic pumps were connected to the cathode and anode effluent ports and used to pump electrolyte through the vertically oriented cell at constant outlet flow rates of 5 mL/min such that the total inlet flow rate was 10 mL/min. The performance of the cathode was evaluated by measuring its potential in 1 M NaCl + X mM $MgCl_2$ (X = 0.0, 1.2, 5, or 120 mM) during electrolysis at constant current density (50 mA/cm^2) for 3 h. The results of these chronopotentiometry (CP) measurements are provided in Fig. 9a, and the average pH of the anode and cathode effluent streams recorded at 3 different times during the CP tests are provided in Fig. 9b. Increasing the concentration of magnesium in the feed stream resulted in higher overpotential losses at the cathode (Fig. 9a), and a less alkaline effluent stream (Fig. 9b). The increased overpotential and lowered cathode effluent pH can be attributed to the formation of $Mg(OH)_2$ according to Eq. (1), which involves the consumption of OH^- generated by the HER (Eq. (6)). However, Fig. 9b shows that a negligible difference in the cathode pH is observed in the presence of 1.2 mM $MgCl_2$ compared to that which is expected from theory based on Eq. (8). Interestingly, a slight improvement in the cathode performance was repeatedly observed for tests carried out in the 1.2 mM $MgCl_2$ electrolyte compared to the Mg-free 1 M NaCl electrolyte. A comparison of polarization curves taken before and after each CP measurement is provided in Fig. S3.

After each set of experiments, the cathode was removed from the electrolyzer and imaged by optical microscopy and SEM. Images of the outside surfaces of the electrodes are shown in Fig. 10. No noticeable deposits of $Mg(OH)_2$ were observed on the samples tested in solutions containing 1.2 mM $MgCl_2$ and 5 mM $MgCl_2$, although some NaCl deposits are observed if electrodes are not washed with water before drying as reflected by the bright regions in the SEM images in Fig. 10d and e. In contrast to the electrodes operated in low Mg^{2+} solutions, the electrode tested in 1 M NaCl + 120 mM $MgCl_2$ was fully coated by solid $Mg(OH)_2$ sludge, which appears as a pasty white substance on the surface of the electrode in Fig. 10c. SEM images and EDS mapping (Fig. S4) corroborated the observations from Fig. 10a, b, and c, where deposits of $Mg(OH)_2$ became more prominent as the concentration of Mg^{2+} increased. As seen in Fig. 10c and f, the $Mg(OH)_2$ deposits thoroughly coat the electrode and result in significant blockage of the pores within the carbon foam electrode. During operation, the accumulating $Mg(OH)_2$deposits can be expected to lead to increasingly large ohmic and concentration overpotentials, resulting in a continual decrease in electrolyzer efficiency. This is consistent with the larger and gradually increasing cathode overpotentials observed in Fig. 9a for the CP measurement carried out in 120 mM Mg^{2+} compared to the stable CP measurements in the 1.2 and 5 mM Mg^{2+} solutions. In addition to decreasing electrolyzer efficiency, pore blockage by $Mg(OH)_2$ can be expected to increase pumping energy requirements due to higher pressure drops required to force fluid flow through increasingly constricted fluidic channels within thein electrode.

The experimental demonstrations in Figs. 9 and 10 illustrate the adverse effects of $Mg(OH)_2$ deposition on/within cathodes when an

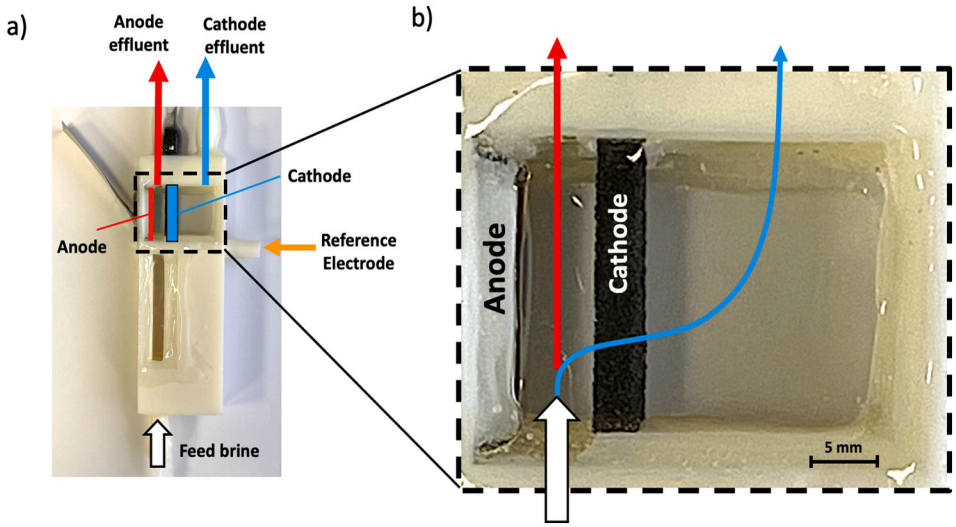

Fig. 8. a) Photograph of the membraneless electrolyzer used in this study. b) Zoomed in view of the center of the cell showing the platinized carbon foam flow-through cathode and platinized titanium foil flow-by anode. The gap distance between the anode and cathode is 5 mm.

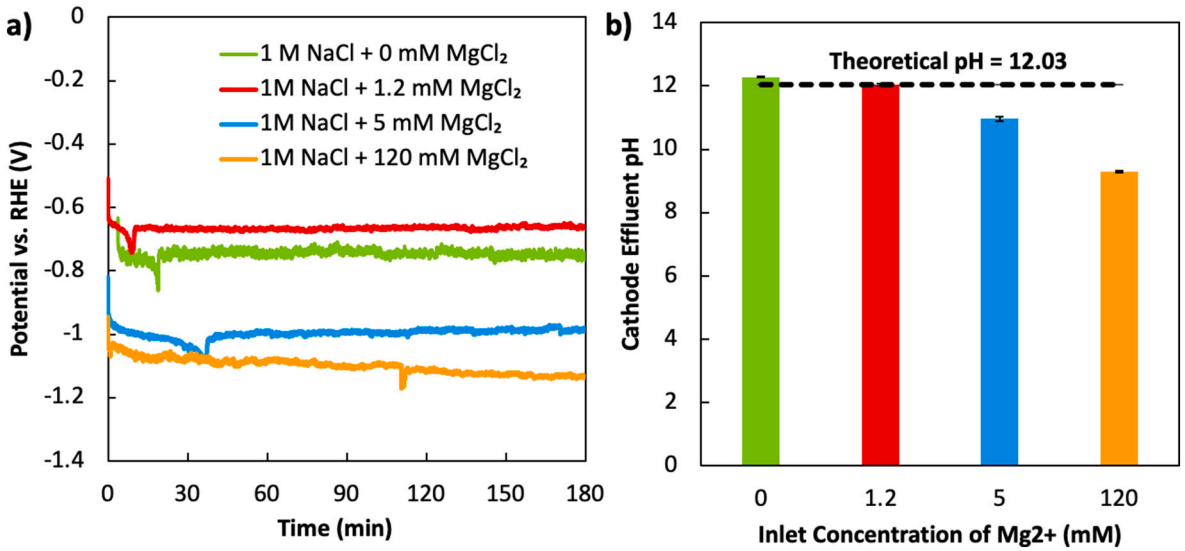

Fig. 9. a) CP stability measurements in 1 M NaCl + 0 mM $MgCl_2$ (green), 1.2 mM $MgCl_2$ (red), 5 mM $MgCl_2$ (blue), and 120 mM $MgCl_2$ (orange) at a constant applied current density of 50 mA/cm^2. Potential vs. RHE was corrected based on the pH of the cathode effluent stream. b) Average pH of product collected from the cathode effluent stream collected at the 45 min, 105 min, and 165 min for each stability test. Error bars in b) are based on 2-sided 95% confidence intervals. The dashed horizontal line represents the theoretical cathode effluent pH based on Eq. (8) assuming that current utilization is 1 and that none of the generated hydroxyls are consumed by Mg^{2+} ions according to Eq. (1). (For interpretation of the references to colour in this figure legend, the reader is referred to the web version of this article.)

electrolyzer is operated in the presence of high Mg^{2+} concentrations. However, these experiments were conducted under very specific operating conditions for a relatively short period of time (3 h) compared to operational periods required for commercial operation. To predict the maximum operating time (t_{max}) before a cathode would experience a maximum allowable amount of precipitated $Mg(OH)_2$ (N_{max}), a simple mathematical model was developed. As detailed below, this model can specifically be used to predict how t_{max} varies as a function of the inlet concentration of Mg^{2+}, the applied current density (i), and the superficial velocity of electrolyte passing through the electrode. In this analysis, N_{max} is normalized by the geometric area of the electrode such that it has units of moles $Mg(OH)_2$ per cm^2 of electrode. As a basis for these calculations, N_{max} = 2.8 mmol/cm^2 was chosen to be the maximum allowable amount of $Mg(OH)_2$ precipitation, which corresponds to the amount of $Mg(OH)_2$ that precipitated during the 3-hour stability test conducted at 50 mA/cm^2 in the 1 M NaCl + 120 mM $MgCl_2$ electrolyte in this study. It was assumed that beyond this level of $Mg(OH)_2$ deposition device operation becomes too inefficient and require maintenance, most likely in the form of treatment by acidified electrolyte to remove the Mg $(OH)_2$ scaling.

For steady-state, constant current density operation of the electrolyzer, t_{max} is given by the ratio of N_{max} to the areal molar rate of Mg $(OH)_2$ precipitation (mole/(s•cm^2)), $r_{Mg(OH)2}$:

$$t_{max} = \frac{N_{max}}{r_{Mg(OH)_2}} \tag{9}$$

Since the $Mg(OH)_2$ precipitation reaction has fast kinetics and is highly favored at the high pH generated at the cathode, the rate of Mg $(OH)_2$ precipitation easily becomes limited by the rate at which the limiting reactant, either Mg^{2+} or OH^-, is introduced to a reactive control

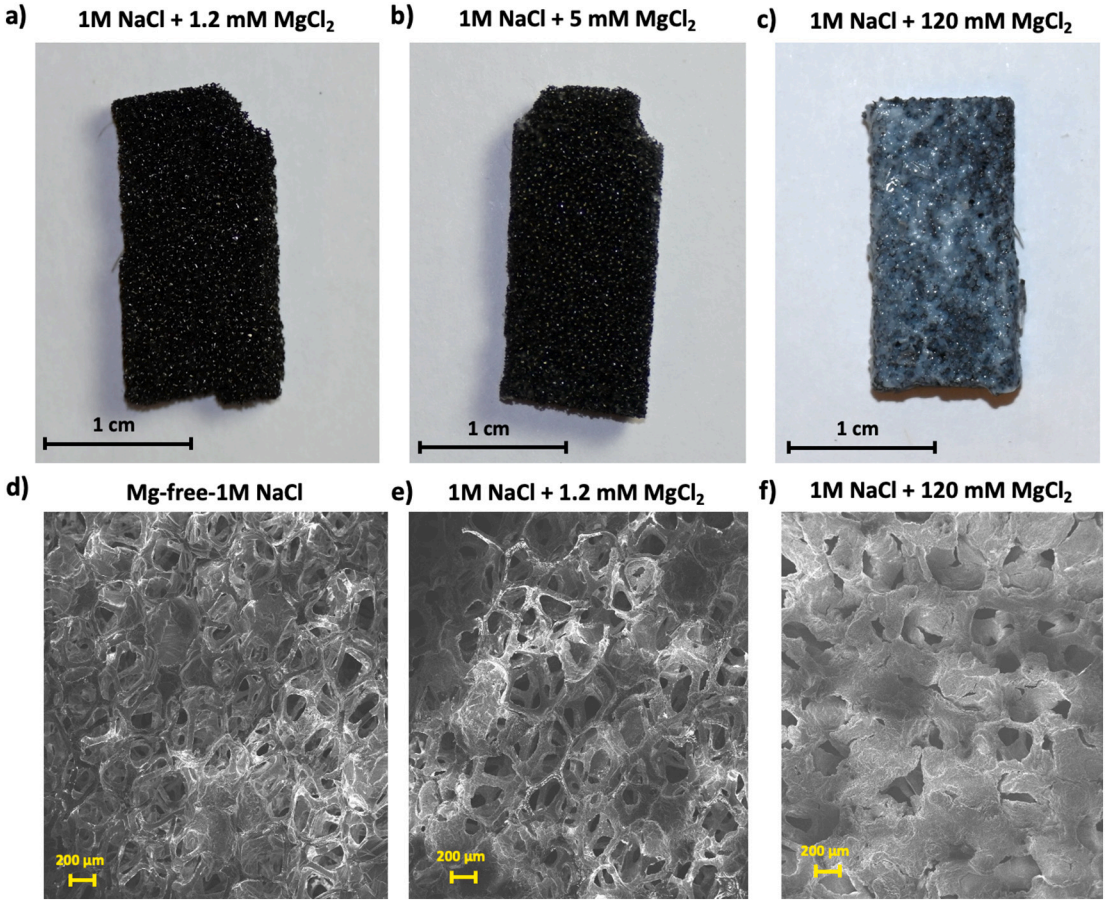

Fig. 10. Outer surfaces of cathodes photographed after 3 h constant current (50 mA/cm^2) stability tests performed in a) 1 M NaCl + 1.2 mM $MgCl_2$, b) 1 M NaCl + 5 mM $MgCl_2$, c) 1 M NaCl + 120 mM $MgCl_2$ electrolytes. SEM Images of cathodes tested in d) Mg-free 1 M NaCl, e) 1 M NaCl + 1.2 mM $MgCl_2$, and f) 1 M NaCl + 120 mM $MgCl_2$.

volume. In this work, $Mg(OH)_2$ precipitation occurs in the porous cathode and cathode effluent chamber where electrochemically generated OH^- reacts with Mg^{2+} contained within the inlet brine. Thus, $r_{Mg(OH)2}$ depends highly on the molar flux of Mg^{2+} entering the cathode ($F_{Mg2+,\ in}$ = mole/s·cm^2) and the areal rate of OH^- generation at the cathode (r_{OH-}), where the former is determined from the cathode inlet volumetric flow rate (v_c) and concentration of Mg^{2+} and the latter is determined from Faraday's law of electrolysis. When $r_{OH-} \ll F_{Mg2+,\ in}$, the rate of $Mg(OH)_2$ precipitation becomes limited by the rate of OH^- generation:

$$OH^- - \text{limited precipitation} : r_{Mg(OH)2} = \frac{r_{OH^-}}{2} = \frac{-i}{2 \cdot n \cdot F} \quad (10)$$

where $n = 1$ mol e$^-$ per mole OH^- and F is the Faraday Constant (F = 96,485C/mol e$^-$). When $F_{Mg2+,\ in} \ll r_{OH-}$, Mg^{2+} is the limiting reactant, resulting in 100% conversion of Mg^{2+} into $Mg(OH)_2$ that is limited by the rate of Mg^{2+} entering the porous cathode:

$$Mg^{2+} - \text{limited precipitation} : r_{Mg(OH)_2} = F_{Mg^{2+},in} = \frac{v_c \cdot C_{Mg,in}}{A_c} \quad (11)$$

where A_c is the area of the cathode and $C_{Mg,\ in}$ is the concentration of Mg^{2+} present in the inlet stream entering the cathode. By comparing the values of r_{OH-} and $F_{Mg2+,\ in}$ used in the experiments carried out in this work, Mg^{2+} was the limiting reactant for experiments carried out in 1.2 and 5 mM $MgCl_2$, while OH^- was the limiting reactant for the experiment carried out at 120 mM $MgCl_2$. This assessment is validated based on the experimentally recorded cathode effluent pH values, which were used to determine how much OH^-, and therefore how much Mg^{2+}, was consumed through $Mg(OH)_2$ precipitation. These calculations reveal that ≈61% and ≈100% of Mg^{2+} was precipitated for the experiment carried out 120 mM $MgCl_2$ and 5 mM $MgCl_2$, respectively. The % of Mg^{2+} precipitated in the experiment run in 1.2 mM $MgCl_2$ could not be reliably determined from the measured cathode effluent pH due to its proximity to the theoretical pH value in the absence of precipitation but can be assumed to be close to 100% given the high pH at the cathode and fact that nearly 100% of Mg^{2+} was precipitated when 5 mM $MgCl_2$ was used.

Using Eqs. (10) and (11), predicted values of t_{max} were calculated for a wide range of operating conditions, with the results shown in Fig. 11. Fig. 11a shows t_{max} as a function of $C_{Mg,in}$ for different operating current densities while holding the inlet fluid velocity constant at 0.042 cm/s. At low $C_{Mg,in}$ (<1 mM), t_{max} is seen to vary inversely with $C_{Mg,in}$ and to be independent of current density since the precipitation reaction is limited by Mg^{2+} according to Eq. (11). However, as $C_{Mg,in}$ increases, the time to reach N_{max} eventually plateaus because OH^- becomes the limiting reactant. Under these OH^--limiting conditions, t_{max} depends entirely on current density, with increases in current density decreasing t_{max}. In Fig. 11b, the effect of varied fluid velocity (or alternately, the volumetric flow rate) on t_{max} was explored by calculating t_{max} as a function of $C_{Mg,in}$ for constant current density of 50 mA/cm^2. Consistent with intuition, Fig. 11b shows that increasing the fluid velocity shifts the transition between Mg^{2+}-limited reaction (diagonal portion of curves) to OH^- limited reaction (horizontal portion of curves) to lower Mg^{2+} concentrations, since higher fluid velocities/flow rates correspond to a higher flux of Mg^{2+} to the cathode surface for a given $C_{Mg,in}$.

Importantly, Fig. 11 can serve as a useful guide for predicting how

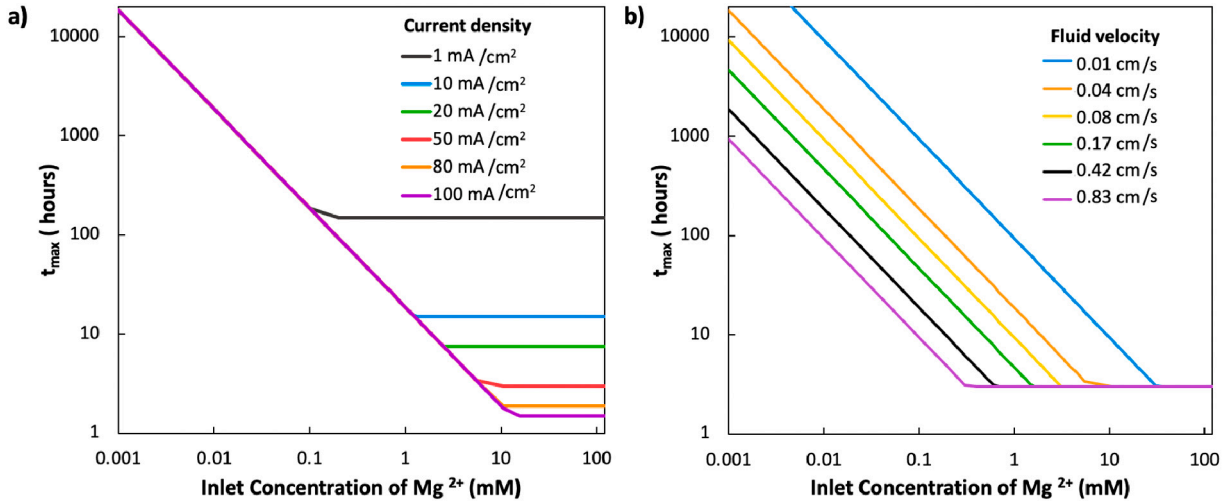

Fig. 11. Predicted operating times before a maximum allowable amount of $Mg(OH)_2$ has precipitated on the cathode or in the catholyte (t_{max}). As a basis for these calculations, the maximum allowable amount of precipitated $Mg(OH)_2$ was chosen to be 2.8 mmol/cm^2, which coincides to the total amount of $Mg(OH)_2$ precipitated on the cathode shown in Fig. 10c and f. In a) t_{max} was calculated as a function of the inlet concentration of Mg^{2+} for different operating current densities and a constant inlet cathodic flow rate of 5 mL/min and constant area of 2 cm^2 (fluid velocity = 0.042 cm/s). In b), t_{max} was calculated as a function of the inlet concentration of Mg^{2+} for different inlet fluid velocities and constant current density of 50 mA/cm^2.

electrolyzer operating conditions can be expected to influence the amount of time that an electrolyzer can be operated in the presence of Mg^{2+} before the cathode needs to be serviced to remove the $Mg(OH)_2$ deposits. For perspective, the membranes of reverse osmosis (RO) desalination units usually need to be descaled once per week. If periodic maintenance were similarly performed on electrolyzers to remove $Mg(OH)_2$ from the cathodes, the analysis in Fig. 11 suggests that low inlet concentrations of Mg^{2+} (<1 mM) should be maintained and that superficial velocities of brine passing through the cathode should be minimized (<0.01 cm/s). Thus, the Mg^{2+} removal achieved under optimal conditions identified in the first part of this study may be sufficient to enable membraneless electrolyzer operation for significant periods of time between descaling maintenance is required.

It should be noted that this study focused on a model brine solution containing Mg^{2+} and NaCl because Mg^{2+} is the metal impurity (excluding Na^+ and K^+) with highest concentration in typical reject brine solution and is known for its ability to create scaling issues on cathode surfaces. However, it is important to acknowledge that there are other species present in brine solutions that will also need to be considered for large-scale implementation of the proposed process. In particular, Ca^{2+} ions and organic molecules are two impurities that could potentially cause issues for electrode operation. Ca^{2+}, like Mg^{2+}, is an alkaline earth metal ion that similarly precipitates as a solid metal hydroxide ($Ca(OH)_2$) by reacting with OH^- at elevated pH. Thus, there is also a risk of $Ca(OH)_2$ deposition on the cathode of a membraneless electrolyzer, but like Mg^{2+}, it is possible to remove Ca^{2+} upstream of the electrolyzer as $Ca(OH)_2$ before it can deposit on the cathode. Fortunately, the concentration of Ca^{2+} within brine is around one-third of the concentration of Mg^{2+} [17], meaning that the removal of Ca^{2+} from reject brine should only lead to an incremental increase in the energy required to produce OH^- used to precipitate it as $Ca(OH)_2$. Interestingly, Ca^{2+} can also be directly removed from the brine by purging the solution with CO_2, which causes the Ca^{2+} to precipitate as calcite ($CaCO_3$) [41,42].

The impact of organic molecules within the brine solution on the performance of a membraneless electrolyzer is harder to gauge. It is well-known in the field of electrochemistry that various organic contaminants within an electrolyte can decrease electrocatalyst performance by fouling or blocking active sites, although rarely does organic content completely deactivate an electrode. It is worth noting that electrochlorination reactors are well-established membrane-free electrolysis cells that can operate for one or more years at a time without maintenance despite the electrodes being in direct contact with organic-laden seawater during operation [43]. Additionally, it is possible to limit the impacts of organic content and other harmful impurities on electrocatalyst performance by encapsulating active electrocatalysts in semi-permeable oxide coatings that allow for reactants and products for the desired hydrogen and oxygen evolution reactions to pass through while blocking impurities from reaching the active site [44]. Thus, there are reasons to be optimistic that Ca^{2+} and organic impurities can also be tolerated but will require additional studies to systematically understand and minimize their impacts. The influence of COD and other impurities like Ca^{2+} ions on electrode durability for membraneless electrolyzer will be addressed in future studies.

4. Conclusions and future prospects

A recirculating electrolyte scheme involving the pretreatment of reject brine to remove magnesium before introducing it as a feed for membraneless electrolyzer was proposed. The optimal conditions for the removal of magnesium from brine have been investigated using response surface methodology. Three process parameters, namely brine salinity, NaOH dose and temperature were optimized with magnesium removal set as the target response using central composite design. Among the three optimized parameters, NaOH dose and brine salinity appeared to have the most significant effect on the removal of magnesium. An increase in NaOH dose caused an increase in the removal of magnesium due to the availability of more hydroxyl ions which drove the magnesium ions present within the brine to form magnesium hydroxide precipitates. On the other hand, an increase in brine salinity decreased the removal of magnesium since the magnesium content proportionally increased with the brine salinity. Meanwhile, the temperature did not seem to have any significant effect on magnesium removal efficiency. Within the experimental conditions, the methodological model of the central composite design was successfully used to predict the percentage of Mg^{2+} recovered based on the response optimizer output. It was concluded that the optimal conditions to remove 98.8% of magnesium were at a brine salinity of 73.5 g/L, NaOH dose of 8.22 g/Land a temperature of 45.5 °C. Characterization of the solid precipitate by XRD, EDS and TGA analysis indicated the generation of high-purity magnesium hydroxide under these optimal conditions.

Upon establishing the capability to remove 98.8% of Mg^{2+} ions from

reject brine, the low-Mg-content electrolyte was fed to membraneless electrolyzers to assess the Mg^{2+} tolerance of the cathode during model brine electrolysis experiments. Platinized carbon foam flow-through electrodes were fabricated and incorporated into a simple membraneless electrolyzer test platform to serve as the cathode, while platinized titanium foil counter electrode served as the anode in an opposing face-to-face configuration. The stability of the cathode was then monitored in 1 M NaCl with varying concentrations of $MgCl_2$ during constant operating current density of 50 mA/cm^2 for 3 h and constant volumetric flow rates of brine through the cell. Based on the chronopotentiometry (CP) measurements and the imaging of cathode cells, it can be concluded that brine solutions with Mg^{2+} concentrations below 5 mM can be used for time periods of at least 3 h as a feed stream for membraneless electrolyzers to produce acids and bases without any noticeable build-up of $Mg(OH)_2$ deposits. Using a mathematical model, this study also establishes the relationships between electrolyzer operating conditions and the time required to deposit a maximum allowable amount of $Mg(OH)_2$ on the cathode surface. For operation in 1.2 mM Mg^{2+} at 5 mL/min and 50 mA/cm^2, the model predicts that the cathode would become coated with 2.8 mmol $Mg(OH)_2$/cm^2 (i.e. similar to the amount deposited in Fig. 10c, f) after 16 h. This analysis highlights the significant benefits that incorporation of the Mg-removal pretreatment step can have on extending the operating time of the electrolyzer before it needs to be temporarily shut down for descaling maintenance. It is worth noting that the impact of calcium ions and other contaminants such as natural organic matters on the membraneless electrolyzer will be considered in a future study.

CRediT authorship contribution statement

Nafis Mahmud, Daniela V. Fraga Alvarez, Muftah El-Naas, Daniel Esposito: Conceptualization, Methodology, Software Nafis Mahmud, Daniela V. Fraga Alvarez, Mohamed Ibrahim: Data curation, Writing-Original draft preparation. Nafis Mahmud, Daniela V. Fraga Alvarez, Mohamed Ibrahim: Visualization, Investigation. Muftah El-Naas, Daniel Esposito: Supervision. Nafis Mahmud, Daniela V. Fraga Alvarez, Mohamed Ibrahim, Muftah El-Naas, Daniel Esposito: Writing- Reviewing and Editing.

Declaration of competing interest

The authors declare the following financial interests/personal relationships which may be considered as potential competing interests: The authors declare the following competing financial interest(s): Daniel Esposito is a co-founder of sHYp, B.V.

Acknowledgment

The authors would like to acknowledge the support of Qatar National Research Fund (a member of Qatar Foundation) through Grant # NPRP 12S-0215-190090. The findings achieved herein are solely the responsibility of the authors. The authors also acknowledge the co-funding provided by Qatar Shell Research and Technology Centre. EDS analysis was carried out at the Central Laboratories unit (CLU), Qatar University. Special thanks to Mr. Sumit Verma (Shell Technology Center, Houston) for his valuable feedback. Open access funding is provided by the Qatar National Library.

Appendix A. Supplementary data

Supplementary data to this article can be found online at https://doi.org/10.1016/j.desal.2021.115489.

References

[1] J. Morillo, J. Usero, D. Rosado, H. El Bakouri, A. Riaza, F.-J. Bernaola, Comparative study of brine management technologies for desalination plants, Desalination 336 (2014) 32–49, https://doi.org/10.1016/j.desal.2013.12.038.
[2] E. Jones, M. Qadir, M.T.H. van Vliet, V. Smakhtin, S.-M. Kang, The state of desalination and brine production: a global outlook, Sci. Total Environ. 657 (2019) 1343–1356, https://doi.org/10.1016/j.scitotenv.2018.12.076.
[3] A. Giwa, V. Dufour, F. Al Marzooqi, M. Al Kaabi, S.W. Hasan, Brine management methods: recent innovations and current status, Desalination 407 (2017) 1–23, https://doi.org/10.1016/j.desal.2016.12.008.
[4] M.H. El-Naas, Reject brine management, in: Desalination, Trends and Technologies, 2011, pp. 237–252.
[5] M.O. Mavukkandy, C.M. Chabib, I. Mustafa, A. Al Ghaferi, F. AlMarzooqi, Brine management in desalination industry: from waste to resources generation, Desalination 472 (2019) 114187, https://doi.org/10.1016/j.desal.2019.114187.
[6] Y. Zhao, J. Wang, Z. Ji, J. Liu, X. Guo, J. Yuan, A novel technology of carbon dioxide adsorption and mineralization via seawater decalcification by bipolar membrane electrodialysis system with a crystallizer, Chem. Eng. J. 381 (2020), 122542, https://doi.org/10.1016/j.cej.2019.122542.
[7] C. Fernandez-Gonzalez, A. Dominguez-Ramos, R. Ibañez, A. Irabien, Electrodialysis with bipolar membranes for valorization of brines, Sep. Purif. Rev. 45 (4) (2016) 275–287, https://doi.org/10.1080/15422119.2015.1128951.
[8] S. Dresp, F. Dionigi, M. Klingenhof, P. Strasser, Direct electrolytic splitting of seawater: opportunities and challenges, ACS Energy Lett. 4 (4) (2019) 933–942, https://doi.org/10.1021/acsenergylett.9b00220.
[9] M. Herrero-Gonzalez, P. Diaz-Guridi, A. Dominguez-Ramos, A. Irabien, R. Ibañez, Highly concentrated HCl and NaOH from brines using electrodialysis with bipolar membranes, Sep. Purif. Technol. 242 (2020), 116785, https://doi.org/10.1016/j.seppur.2020.116785.
[10] S. Lakshmanan, T. Murugesan, The chlor-alkali process: work in progress, Clean Technol. Environ. Policy 16 (2) (2014) 225–234, https://doi.org/10.1007/s10098-013-0630-6.
[11] H. Strathmann, Electrodialysis, a mature technology with a multitude of new applications, Desalination 264 (3) (2010) 268–288, https://doi.org/10.1016/j.desal.2010.04.069.
[12] M. Sadrzadeh, T. Mohammadi, Treatment of sea water using electrodialysis: current efficiency evaluation, Desalination 249 (1) (2009) 279–285, https://doi.org/10.1016/j.desal.2008.10.029.
[13] O.O. Talabi, A.E. Dorfi, G.D. O'Neil, D.V. Esposito, Membraneless electrolyzers for the simultaneous production of acid and base, Chem. Commun. 53 (57) (2017) 8006–8009, https://doi.org/10.1039/C7CC02361H.
[14] G.D. O'Neil, C.D. Christian, D.E. Brown, D.V. Esposito, Hydrogen production with a simple and scalable membraneless electrolyzer, J. Electrochem. Soc. 163 (11) (2016) F3012–F3019, https://doi.org/10.1149/2.0021611jes.
[15] J.T. Davis, J. Qi, X. Fan, J.C. Bui, D.V. Esposito, Floating membraneless PV-electrolyzer based on buoyancy-driven product separation, Int. J. Hydrog. Energy 43 (3) (2018) 1224–1238, https://doi.org/10.1016/j.ijhydene.2017.11.086.
[16] P. Badjatya, A.H. Akca, D.V.F. Alvarez, B. Chang, S. Ma, X. Pang, E. Wang, Q. V. Hinsberg, D.V. Esposito, S. Kawashima, CO2-negative cement manufacturing from seawater-derived feedstocks, in: ChemRxiv, Cambridge Open Engage, 2021, https://doi.org/10.33774/chemrxiv-2021-5dznt-v2. Submitted for publication.
[17] A.F. Mohammad, M.H. El-Naas, A.H. Al-Marzouqi, M.I. Suleiman, M.Al Musharfy, Optimization of magnesium recovery from reject brine for reuse in desalination post-treatment, J. Water Process Eng. 31 (2019), 100810, https://doi.org/10.1016/j.jwpe.2019.100810.
[18] S. Ruan, E.-H. Yang, C. Unluer, Production of reactive magnesia from desalination reject brine and its use as a binder, J. CO2 Utilization 44 (2021), 101383, https://doi.org/10.1016/j.jcou.2020.101383.
[19] A. Roine, HSC - SOFTWARE VER. 3.0 FOR THERMODYNAMIC CALCULATIONS, in: W.T. Thompson, F. Ajersch, G. Eriksson (Eds.), Proceedings of the International Symposium on Computer Software in Chemical and Extractive Metallurgy, Pergamon, Oxford, 1989, pp. 15–29, https://doi.org/10.1016/B978-0-08-036087-4.50007-0.
[20] E.A. Atekwana, E.A. Atekwana, R.S. Rowe, D.D. Werkema, F.D. Legall, The relationship of total dissolved solids measurements to bulk electrical conductivity in an aquifer contaminated with hydrocarbon, J. Appl. Geophys. 56 (4) (2004) 281–294, https://doi.org/10.1016/j.jappgeo.2004.08.003.
[21] R.L. Mason, R.F. Gunst, J.L. Hess, Statistical Design and Analysis of Experiments: With Applications to Engineering and Science, John Wiley & Sons, 2003.
[22] G.E. Box, N.R. Draper, Empirical Model-Building and Response Surfaces, Wiley, New York, 1987.
[23] M.A. Bezerra, R.E. Santelli, E.P. Oliveira, L.S. Villar, L.A. Escaleira, Response surface methodology (RSM) as a tool for optimization in analytical chemistry, Talanta 76 (5) (2008) 965–977, https://doi.org/10.1016/j.talanta.2008.05.019.
[24] D. Baş, İ.H. Boyacı, Modeling and optimization I: usability of response surface methodology, J. Food Eng. 78 (3) (2007) 836–845, https://doi.org/10.1016/j.jfoodeng.2005.11.024.
[25] J. Antony, 6 - full factorial designs, in: J. Antony (Ed.), Design of Experiments for Engineers and Scientists, Second edition, Elsevier, Oxford, 2014, pp. 63–85, https://doi.org/10.1016/B978-0-08-099417-8.00006-7.
[26] D.F. van der Vliet, C. Wang, D. Li, A.P. Paulikas, J. Greeley, R.B. Rankin, D. Strmcnik, D. Tripkovic, N.M. Markovic, V.R. Stamenkovic, Unique electrochemical adsorption properties of Pt-skin surfaces, Angew. Chem. Int. Ed. 51 (13) (2012) 3139–3142, https://doi.org/10.1002/anie.201107668.

[27] H. Dong, C. Unluer, E.-H. Yang, A. Al-Tabbaa, Recovery of reactive MgO from reject brine via the addition of NaOH, Desalination 429 (2018) 88–95, https://doi.org/10.1016/j.desal.2017.12.021.
[28] H. Dong, E.-H. Yang, C. Unluer, F. Jin, A. Al-Tabbaa, Investigation of the properties of MgO recovered from reject brine obtained from desalination plants, J. Clean. Prod. 196 (2018) 100–108, https://doi.org/10.1016/j.jclepro.2018.06.032.
[29] M.S. Thabit, A.H. Hawari, M.H. Ammar, S. Zaidi, G. Zaragoza, A. Altaee, Evaluation of forward osmosis as a pretreatment process for multi stage flash seawater desalination, Desalination 461 (2019) 22–29, https://doi.org/10.1016/j.desal.2019.03.015.
[30] R. Borsani, S. Rebagliati, Fundamentals and costing of MSF desalination plants and comparison with other technologies, Desalination 182 (1) (2005) 29–37, https://doi.org/10.1016/j.desal.2005.03.007.
[31] S. Yousefi, B. Ghasemi, M. Tajally, A. Asghari, Optical properties of MgO and Mg(OH)2 nanostructures synthesized by a chemical precipitation method using impure brine, J. Alloys Compd. 711 (2017) 521–529, https://doi.org/10.1016/j.jallcom.2017.04.036.
[32] L. Mo, M. Deng, M. Tang, Effects of calcination condition on expansion property of MgO-type expansive agent used in cement-based materials, Cem. Concr. Res. 40 (3) (2010) 437–446, https://doi.org/10.1016/j.cemconres.2009.09.025.
[33] J.K. Bartley, C. Xu, R. Lloyd, D.I. Enache, D.W. Knight, G.J. Hutchings, Simple method to synthesize high surface area magnesium oxide and its use as a heterogeneous base catalyst, Appl. Catal. B Environ. 128 (2012) 31–38, https://doi.org/10.1016/j.apcatb.2012.03.036.
[34] S. Purwajanti, L. Zhou, Y.Ahmad Nor, J. Zhang, H. Zhang, X. Huang, C. Yu, Synthesis of Magnesium Oxide Hierarchical Microspheres: A Dual-Functional Material for Water Remediation, ACS Applied Materials & Interfaces 7 (38) (2015) 21278–21286, https://doi.org/10.1021/acsami.5b05553.
[35] G. Jauffret, J. Morrison, F.P. Glasser, On the thermal decomposition of nesquehonite, J. Therm. Anal. Calorim. 122 (2) (2015) 601–609, https://doi.org/10.1007/s10973-015-4756-0.
[36] L.A. Hollingbery, T.R. Hull, The thermal decomposition of huntite and hydromagnesite—a review, Thermochim. Acta 509 (1) (2010) 1–11, https://doi.org/10.1016/j.tca.2010.06.012.
[37] I. Halikia, P. Neou-Syngouna, D. Kolitsa, Isothermal kinetic analysis of the thermal decomposition of magnesium hydroxide using thermogravimetric data, Thermochim. Acta 320 (1–2) (1998) 75–88, https://doi.org/10.1016/S0040-6031(98)00413-4.
[38] D.W. Kirk, A.E. Ledas, Precipitate formation during sea water electrolysis, Int. J. Hydrog. Energy 7 (12) (1982) 925–932, https://doi.org/10.1016/0360-3199(82)90160-4.
[39] E. Baniasadi, I. Dincer, G.F. Naterer, Electrochemical analysis of seawater electrolysis with molybdenum-oxo catalysts, Int. J. Hydrog. Energy 38 (6) (2013) 2589–2595, https://doi.org/10.1016/j.ijhydene.2012.11.106.
[40] X. Lu, J. Pan, E. Lovell, T.H. Tan, Y.H. Ng, R. Amal, A sea-change: manganese doped nickel/nickel oxide electrocatalysts for hydrogen generation from seawater, Energy Environ. Sci. 11 (7) (2018) 1898–1910, https://doi.org/10.1039/C8EE00976G.
[41] B.S. Lalia, A. Khalil, R. Hashaikeh, Selective electrochemical separation and recovery of calcium and magnesium from brine, Sep. Purif. Technol. 264 (2021), 118416, https://doi.org/10.1016/j.seppur.2021.118416.
[42] B.S. Lalia, R. Hashaikeh, Electrochemical precipitation to reduce waste brine salinity, Desalination 498 (2021), 114796, https://doi.org/10.1016/j.desal.2020.114796.
[43] C. Ray, R. Jain, Chapter 4 - disinfection systems, in: C. Ray, R. Jain (Eds.), Low Cost Emergency Water Purification Technologies, Butterworth-Heinemann, Oxford, 2014, pp. 55–86, https://doi.org/10.1016/B978-0-12-411465-4.00004-4.
[44] N.Y. Labrador, E.L. Songcuan, C. De Silva, H. Chen, S.J. Kurdziel, R. K. Ramachandran, C. Detavernier, D.V. Esposito, Hydrogen evolution at the buried interface between Pt thin films and silicon oxide nanomembranes, ACS Catal. 8 (3) (2018) 1767–1778, https://doi.org/10.1021/acscatal.7b02668.